Excited State Electron Transfer from Ru(II) Polypyridyl Complexes Anchored to Nanocrystalline TiO_2 through Rigid-Rod Linkers

Dong Wang, Richard Mendelsohn, and Elena Galoppini*

Chemistry Department, Rutgers University, 73 Warren Street, Newark, New Jersey 07102

Paul G. Hoertz, Rachael A. Carlisle, and Gerald J. Meyer*

Department of Chemistry and Department of Materials Science and Engineering, Johns Hopkins University, 3400 North Charles Street, Baltimore, Maryland 21218

Received: June 12, 2004; In Final Form: August 10, 2004

Rigid-rod linkers varying in length were used to bind Ru(II) polypyridyl complexes to the surface of TiO_2 (anatase) and of ZrO_2 nanoparticle thin films. The linkers were made of *p*-phenyleneethynylene $(Ph\text{-}E)_n$ bridges carrying two COOR anchoring groups at the end and were capped with Ru(II) polypyridyl complexes as the sensitizing chromophores. Two series of rigid-rod sensitizers were prepared: Ru complexes having bpy or 4,4′-$(Cl)_2$-bpy as the ancillary ligands. In the first series, the excited state was localized on the rigid-rod linker, in the second series, the excited states were localized on the 4,4′-$(Cl)_2$-bpy ligands. The rigid-rod sensitizers with $Ru(bpy)_2$ complexes did bind strongly ($K_{ad} \sim 10^5\ M^{-1}$) with high surface coverages ($\sim 10^{-8}$ mol/cm^2) on the nanostructured metal oxide films, ZrO_2 and anatase TiO_2. The length of the fully conjugated rigid-rod linker influences the photophysical properties of the sensitizer, and nanosecond transient absorption measurements indicated long-lived metal-to-ligand charge-transfer (MLCT) excited states ($\sim 2\ \mu s$) with evidence for delocalization onto the rigid-rod linker. The interfacial electron transfer behavior on TiO_2 was found to be dependent on the Brønsted acidity or basicity of the surface. On base pretreated TiO_2, the excited state electron injection yields were low and could be increased by addition of $LiClO_4$ to an external CH_3CN solution. Under these conditions, a fraction of the injection process could be time resolved on a 10 ns time scale. On acidic TiO_2, ultrafast excited state electron injection was observed for both series. Recombination was found to be second order with average rate constants independent of which rigid-rod sensitizer was excited. For rigid-rod sensitizers with $Ru(4,4'\text{-}(Cl)_2\text{-}bpy)_2$, there was evidence for a direct interaction between the 4,4′-$(Cl)_2$-bpy ligands and the TiO_2 surface. Photophysical and interfacial electron transfer properties of these Cl-substituted complexes were nearly independent of the rigid-rod length.

Introduction

Polypyridine complexes of Ru(II) are classical photosensitizing dyes or "sensitizers" for nanocrystalline TiO_2 (Grätzel) solar cells.[1,2] The sensitizers are bound to anatase TiO_2 nanoparticles through anchoring functional groups, such as carboxylic acid or phosphonate groups, on the diimine ligand,[1a] and the development of rigid molecular linkers to the surface is attracting increasing attention.[3] Rigid linkers varying in length and structure that have the shape of tripods were developed in our laboratories to study interfacial charge injection processes, Figure 1.[4] Tripodal sensitizers, because of the three-point attachment, stand perpendicularly to the surface and were useful in studies that required a well-defined binding geometry and distance of the sensitizer (S) from the semiconductor.[5,6] There was evidence that the conjugated bridge (b) played a role in the injection process,[6] but the tetrahedral core (carbon or adamantane) was likely to act as an insulating unit.

An alternative to tripodal linkers was to use rigid-rod linkers that provided a fully conjugated bridge to the surface.[7] We have recently communicated studies of rigid-rods substituted with pyrene sensitizers and two COOH anchoring groups.[8] Light absorption by pyrene resulted in quantitative, sub-nanosecond, electron injection into the TiO_2 nanoparticles. Interestingly, the

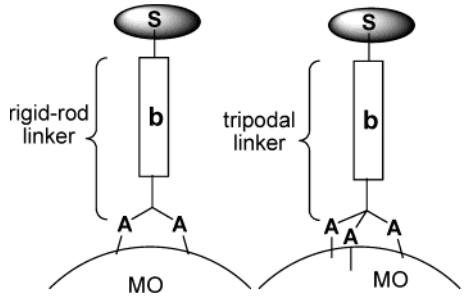

Figure 1. Schematic illustration of rigid-rod and tripodal linkers bound to metal oxide (MO) nanoparticles' surface consisting of a bridge (b) of variable length, anchoring groups (A), and a sensitizing dye (S).

conjugated *p*-phenyleneethynylene, $(Ph\text{-}E)_n$, bridge of the rigid-rods considerably enhanced the pyrene extinction coefficient and red shifted the absorption spectrum. Thus, the photon-to-electron conversion efficiency at single wavelengths of light was a function of the bridge length and could be controlled at the molecular level for optoelectronic applications. However, for regenerative solar cell applications, Ru(II) polypyridine complexes are generally preferred to organic chromophores because of their visible light harvesting efficiency, tunability, and stability.[1a,2]

10.1021/jp047454t CCC: $27.50
Published on Web 10/01/2004

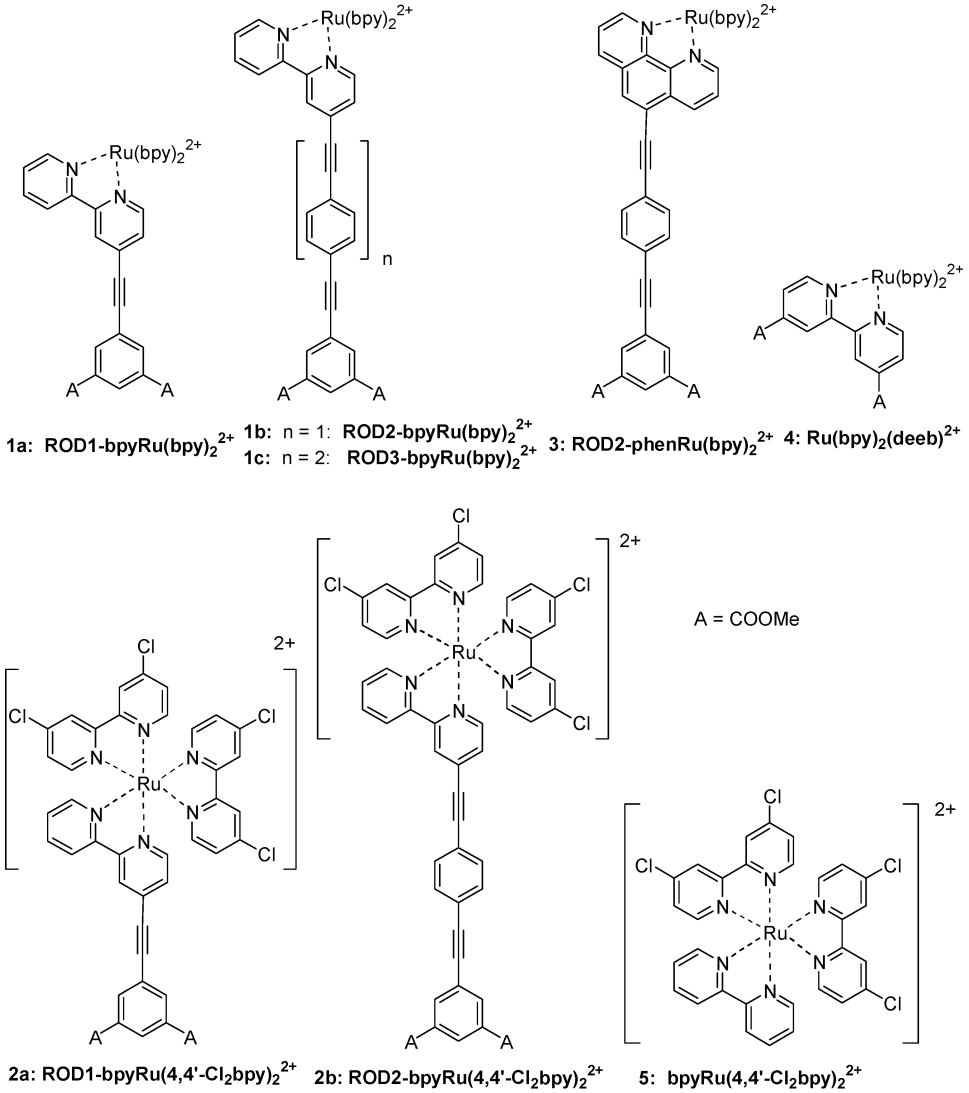

Figure 2. Structure of rigid-rod complexes and two reference complexes. The rigid-rod linkers are made of $(Ph\text{-}E)_n$ units and are terminated with two methyl esters (COOMe) as the anchoring groups (A). The number after ROD in the abbreviated name refers to the number of Ph-E units in the linker. The counterion was PF_6^- in all cases.

In this paper, we describe the synthesis and studies of two series of rigid-rod linkers varying in length and substituted with Ru complexes, Figure 2. In the first series (**1a**−**c** and **3**), the ancillary ligands are bpy for the Ru complexes; in the second series (**2a**−**b**) the ancillary ligands are 4,4′-$(Cl)_2$-bpy, Figure 2. The studies were performed on the compounds in solution as well as anchored to nanocrystalline TiO_2 or ZrO_2 thin films. A prime motivation for these studies was to ascertain whether tuning the sensitizer−nanoparticle electronic interactions by varying the distance could be used to control the rate constants for charge injection and/or recombination.[9] More specifically, we wish to find conditions where the injection quantum yield, ϕ_{inj}, was still unity while the charge recombination rate was further inhibited. Such conditions would not be expected to significantly improve efficiencies for optimized sensitizers such as N3, *cis*-$Ru(dcbpy)_2(NCS)_2$. However, these conditions would be useful for "black" sensitizers that have more negative Ru(III/II) reduction potentials such that the rate constants for charge recombination and iodide oxidation are competitive leading to less efficient collection of the injected electrons in the external circuit.[10] To test whether the fully conjugated rigid-rod linker made of $(Ph\text{-}E)_n$ units functions as a conduit for electron transport, we specifically designed compounds where the MLCT excited state was localized on ancillary 4,4′-$(Cl)_2$-bpy ligands, rather than on the rigid-rod. This design did indeed provide us with the opportunity to study "remote" interfacial charge-transfer processes (vide infra).

Since we initiated these studies on the tripodal[4−6] and rigid-rod[7,8] sensitizers, Kilså et al.[11] have reported TiO_2 sensitization studies of rigid-rods of various lengths carrying Ru(II) polypyridyl sensitizers and one COOH anchoring group. The lack of clear distance dependencies suggested that the rods were bound to TiO_2 with multiple orientations and distances with respect to the surface.[11] Although the rigid-rods reported herein are very similar to those previously reported,[11] they differ in several important respects. First, the linkers described here have two anchoring groups instead of one, which may influence the sensitizer−surface binding mode and orientation. Second, the bridge is made of *p*-phenyleneethynylene spacers, $(Ph\text{-}E)_n$, instead of *p*-phenylene units, $(Ph)_n$. The $(Ph\text{-}E)_n$ units, as opposed to $(Ph)_n$, are able to assume a flat, fully conjugated conformation. The degree to which the excited electron is dispersed into the bridge is therefore different, and this could alter both the excited state and the interfacial electron transfer properties. In fact, we found that the photophysical properties of the Ru(II) rigid-rod sensitizers described herein

SCHEME 1. Conditions and Reagents[a]

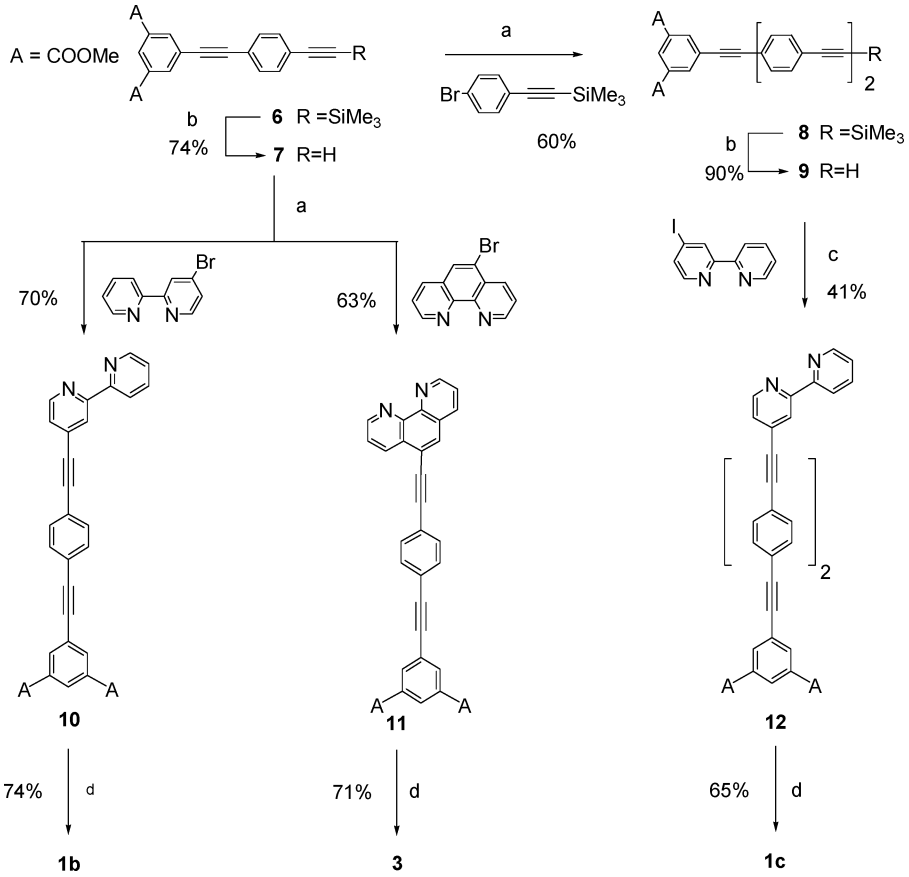

[a] Step a: 1. $(Me_3Si)_2NLi$, MeO-9-BBN, THF; 2. $Pd(PPh_3)_4$. Step b: TBAF, r.t. THF. Step c: $Pd(PPh_3)_4$, CuI, piperidine, r.t. Step d: $(bpy)_2RuCl_2 \cdot 2H_2O$, EtOH, reflux.

shared more commonalties with the oligomeric 4,4′-*p*-phenyleneethynylenes Ru(II) polypyridyl derivatives studied in considerable detail by Schanze[12] for applications in organic light emitting diodes and sensors.

Experimental Section

1. Metal Oxide Thin Films. Transparent and mesoporous thin films of TiO_2 or ZrO_2 on glass slides were prepared in a manner very similar to that previously described.[13] ZrO_2, an insulator (band gap $\approx$ 5 eV),[1a] was used to study the excited state of bound molecules. The films were pretreated with aqueous acid or with aqueous base prior to attachment of the sensitizers.[14] Acid pretreated films were prepared by immersing the films in pH = 1 H_2SO_4 (aq), while basic films were pretreated using pH = 11 NaOH (aq). After this treatment, the films were rinsed with CH_3CN prior to immersion in an $\sim$0.1−1 mM CH_3CN solution of the sensitizer for 24 h. The sensitized films were thoroughly rinsed and then immersed in pure solvent for several hours until desorption of weakly bound sensitizer molecules was no longer detected (UV−vis of the solution).

2. Synthesis. The reagents, experimental methods, and instrumentation used are described in the General Section in the Supporting Information. The syntheses of **1a** and **6** have been published.[7] The synthetic strategy for **1b**, **3**, and **1c** is outlined in Scheme 1. The complexes with Cl-substituted bpy ligands, **2a** and **2b**, were prepared from the same ligands used to synthesize **1a** and **1b** but using $(4,4'\text{-}(Cl)_2\text{-bpy})_2RuCl_2 \cdot 2H_2O$.[15]

*2.1. Synthesis of **7***. TBAF (360 mg, 1.14 mmol) was added to a solution of **6**[7] (400 mg, 1.03 mmol) in THF. After stirring at room temperature for 2 h, water (30 mL) was added, and after standard workup with $CHCl_3$, the crude was purified through column chromatography (hexanes/AcOEt; 9/1, $R_f = 0.3$) to give 240 mg of **7** as a yellow powder (yield: 74%). mp: 160−163 °C. IR (cm^{-1}): 3256 (υ ≡C−H), 2920 (υC−H(aliph.)), 2216 (υC≡C), 1728 (υC═O), 1594 (υC⋯C(Ar)), 1444, 1252. ^1H NMR δ_H ($CDCl_3$): 8.60 (1H, t, J = 1.5, *Ph*COOMe), 8.33 (2H, d, J = 1.5, *Ph*COOMe), 7.47 (4H, s), 3.93 (6H, s, COO*Me*) 3.18 (1H, s, C≡C*H*). ^{13}C NMR δ_C ($CDCl_3$): 165.51 (*C*OOMe), 136.47, 132.12, 131.58, 130.99, 130.22, 124.02, 122.87, 122.51, 90.59, 89.18, 83.07, 79.22, 52.52 (COO*Me*). GC/MS *m*/*z*: 318 (M^+, 100), 287 (M-31, 45), 259 (M-59, 15), 244 (M-74, 25), 200 (M-118, 15), 187 (M-131, 15). HRMS Calcd for $C_{20}H_{14}O_4$: 318.0892. Found: 318.0891.

*2.2. General Procedure for the Synthesis of Rigid-Rod Ligands **8**, **10**, and **11***. Lithium bis(trimethylsilyl)amide (0.74 mmol, 0.74 mL of 1.0 M hexane solution) was added to a solution of **7** (201 mg, 0.632 mmol) in THF (15 mL) at −78 °C. After 30 min, 9-MeO-9-BBN (0.74 mmol, 0.74 mL of 1.0 M hexane solution) was added. The mixture was stirred at −78 °C for 2 h, then transferred via cannula to a second flask containing $Pd(PPh_3)_4$ (36 mg, 0.032 mmol) and 1-bromo-4-trimethylethynylbenzene (196 mg, 0.773 mmol) for **8**, 4-bromo-2,2′-bipyridine (182 mg, 0.773 mmol)[16] for **10**, or 5-bromo-1,10-phenanthroline[17](200 mg, 0.773 mmol) for **11** in THF (15 mL). The reaction mixture was refluxed overnight, then allowed

to cool to room temperature and water (20 mL) was added. After standard workup with chloroform, the crude was purified by silica gel column chromatography (hexanes/AcOEt, 9/1, R_f = 0.2 for **8**; AcOEt/$CHCl_3$, 15/85, R_f = 0.2 for **10**; AcOEt/$CHCl_3$, 1/4, R_f = 0.3 for **11**) to give the corresponding product. **8**: Yield: 60% (186 mg, yellow powder). IR (cm^{-1}): 3084 (υC−H(Ar)), 2924 (υC−H(aliph.)), 2218 (υC≡C), 1730 (υC═O), 1601 (υC⋯C(Ar)), 1440, 1249. ^{1}H NMR δ_H ($CDCl_3$): 8.64 (1H, t, J = 1.5, *Ph*COOMe), 8.37 (2H, d, J = 1.5, *Ph*COOMe), 7.53 (4H, m), 7.46 (4H, m), 3.98 (6H, s, PhCOO*Me*), 0.27 (9H, s, $Si(CH_3)_3$). ^{13}C NMR δ_C ($CDCl_3$): 165.54 (*C*OOMe), 136.47, 131.91, 131.67, 131.59, 131.40, 130.96, 130.19, 124.08, 123.41, 123.17, 122.91, 122.41, 104.51, 96.48, 91.18, 90.85, 90.79, 89.21, 52.55 (COO*Me*), −0.13 ($Si(CH_3)_3$). Anal. Calcd for $C_{31}H_{26}O_4Si$: C, 75.89; H, 5.34; Found: C, 75.96; H, 5.51. **10**: Yield: 70% (209 mg as white powder). mp: 156−158 °C. IR (cm^{-1}): 3027 (υC−H(Ar)), 2211 (υC≡C), 1729 (υC═O), 1601 (υC⋯C(Ar)), 1440, 1245. ^{1}H NMR δ_H ($CDCl_3$): 8.67 (1H, d, J = 4.0), 8.63 (1H, d, J = 5.0), 8.59 (1H, t, J = 2.0), 8.51 (1H, s), 8.38 (1H, d, J = 8.0), 8.32 (2H, d, J = 2.0), 7.80 (1H, td, J_1 = 8.0, J_2 = 2.0), 7.51 (4H, s), 7.35 (1H, dd, J_1 = 5.0, J_2 = 1.5), 7.30 (1H, m), 3.93 (6H, s, COO*Me*). ^{13}C NMR δ_C ($CDCl_3$): 165.45 (*C*OOMe), 156.13, 155.31, 149.15, 149.11, 137.00, 136.44, 132.07, 131.88, 131.72, 130.95, 130.22, 125.15, 124.02, 123.95, 123.16, 123.12, 122.55, 121.14, 93.29, 90.64, 89.53, 89.00, 52.49 (COO*Me*). HRMS calcd for $C_{30}H_{20}O_4N_2$: 472.1423. Found: 472.1424. **11**: Yield: 63% (197 mg, white powder). mp: 242−244 °C. IR (cm^{-1}): 3010 (υC−H(Ar)), 2215 (υC≡C), 1728 (υC═O), 1246, 1002, 827. ^{1}H NMR δ_H ($CDCl_3$): 9.25 (1H, dd, J_1 = 4.5, J_2 = 1.5), 9.21 (1H, dd, J_1 = 4.5, J_2 = 2.0), 8.81 (1H, dd, J_1 = 8.5, J_2 = 2.0), 8.61 (1H, t, J = 1.5), 8.36 (2H, d, J = 1.5), 8.24 (1H, dd, J_1 = 8.5, J_2 = 1.5), 8.09 (1H, s), 7.76 (1H, m), 7.66 (1H, m), 7.61 (4H, m), 3.95 (6H, s, COO*Me*). ^{13}C NMR δ_C ($CDCl_3$): 165.50 (*C*OOMe), 150.50, 150.35, 131.91, 131.88, 131.84, 131.80, 131.76, 131.03, 130.79, 130.30, 128.39, 128.23, 136.84, 136.50, 123.94, 123.88, 123.80, 123.25, 122.65, 120.04, 95.52, 90.60, 89.70, 87.42, 52.60 (COO*Me*). HRMS Calcd for $C_{32}H_{20}O_4N_2$: 496.1423. Found: 496.1414.

*2.3. Synthesis of **9***. Deprotection of **8** by TBAF was performed using same procedure described to prepare **7.** Alkyne **9** was obtained as a yellow powder (yield 90%). IR (cm^{-1}): 3286 (υ≡C−H), 3073 (υC−H(Ar)), 2952 (υC−H(aliph.)), 2211 (υC≡C), 1728 (υC═O), 1599 (υC⋯C(Ar)), 1439, 1246. ^{1}H NMR δ_H ($CDCl_3$): 8.54 (1H, t, J = 1.5, *Ph*COOMe), 8.27 (2H, d, J = 1.5, *Ph*COOMe), 7.44 (4H, m), 7.39 (4H, m), 3.88 (6H, s, COO*Me*), 3.11 (1H, s, C≡C*H*). ^{13}C NMR δ_C ($CDCl_3$): 164.51 (*C*OOMe), 135.45, 131.08, 130.78, 130.68, 130.62, 130.48, 129.98, 129.18, 123.07, 122.37, 121.49, 121.16, 89.98, 89.88, 89.84, 88.26, 82.18, 78.12, 51.53 (COO*Me*).

*2.4. Synthesis of **12***. CuI (10 mg, 0.052 mmol) and $Pd(PPh_3)_4$ (25 mg, 0.022 mmol) were added under argon to a deaerated solution of 4-iodo-2,2′-bipyridine[18] (74 mg, 0.26 mmol) and **10** (107 mg, 0.256 mmol) in piperidine (7 mL). The reaction mixture was stirred overnight at room temperature. The solvent was removed in vacuo and the solid residue was purified by silica gel column ($CHCl_3$/MeOH, 97/3, R_f = 0.2). Compound **12** was obtained as an orange-brown powder (60 mg, yield: 41%). IR (cm^{-1}): 3060 (υC−H(Ar)), 2950 (υC−H(aliph.)), 2205 (υC≡C), 1729 (υC═O), 1582 (υC⋯C(Ar)), 1437, 1245. ^{1}H NMR δ_H ($CDCl_3$): 8.76 (1H, d, J = 4.0), 8.72 (1H, d, J = 5.0), 8.64 (1H, t, J = 2.0), 8.63 (1H, s), 8.53 (1H, d, J = 8.0), 8.38 (2H, d, J = 2.0), 7.92 (1H, ddd, J_1 = J_2 = 8.0, J_3 = 2.0), 7.57 (4H, d, J = 2.0), 7.55 (4H, s), 7.47 (1H, dd, J_1 = 5.0, J_2 = 2.0), 7.41 (1H, m), 3.98 (6H, s, COO*Me*).^{13}C NMR δ_C ($CDCl_3$): 165.50 (*C*OOMe), 156.17, 155.36, 149.18, 149.13, 137.00, 136.44, 131.85, 131.68, 131.63, 130.97, 130.17, 128.51, 128.42, 125.15, 124.06, 124.03, 123.69, 123.30, 123.14, 122.53, 122.22, 121.16, 93.44, 91.25, 91.05, 90.82, 89.28, 88.90, 52.51 (COO*Me*). Anal. Calcd for $C_{38}H_{24}N_2O_4$: C, 79.71; H, 4.22; N, 4.89; Found: C, 77.90; H, 4.52; N, 4.26.

*2.5. General Procedure for the Synthesis of Complexes **1b**, **1c**, and **3***. A solution of **10**, **11**, or **12** (0.329 mmol) in THF (5 mL) was added to ethanol (30 mL). To the solution, deaerated by bubbling nitrogen for 10 min, was added $Ru(bpy)_2Cl_2 \cdot 2H_2O$ (188 mg, 0.362 mmol), and the mixture was refluxed overnight under nitrogen, then cooled to room temperature and filtered. Addition of aqueous $NaPF_6$ (7.70 g, 45.8 mmol) to the filtrate formed precipitate, which was collected and washed with water to afford the complexes as orange powders. **1b**: Yield: 74%. IR (cm^{-1}): 2909 (υC−H(aliph.)), 2206 (υC≡C), 1733 (υC═O), 1249, 1004, 841. ^{1}H NMR δ_H (acetone-d_6): 8.97 (2H, m), 8.84 (4H, m), 8.58 (1H, t, J = 2.0), 8.35 (2H, d, J = 2.0), 8.23 (6H, m), 8.12 (5H m), 7.70 (4H, m), 7.62 (6H, m), 3.98 (6H, s, COO*Me*). ^{13}C NMR δ_C (acetone-d_6): 165.71 (*C*OOMe), 158.60, 158.07, 158.05, 157.98, 157.68, 152.87, 152.82, 152.80, 152.74, 152.64, 139.12, 139.09, 139.01, 136.82, 133.09, 133.07, 132.89, 132.38, 130.77, 129.70, 129.22, 128.84, 126.94, 125.68, 125.37, 124.90, 124.70, 122.58, 97.67, 91.15, 90.56, 88.40, 53.04 (COO*Me*). HRMS Calcd for $C_{50}H_{36}F_{12}N_6O_4P_2Ru$: 1031.1480. Found: 1031.1469. Anal. Calcd for $C_{50}H_{36}F_{12}N_6O_4P_2Ru$: C, 51.07; H, 3.09; N, 7.15; Found: C, 51.32; H, 3.13; N, 6.93. **3**: Yield: 71%. IR (cm^{-1}): 2210 (υC≡C), 1730 (υC═O), 1250, 1016, 842. ^{1}H NMR δ_H (acetone-d_6): 9.19 (1H, dd, J_1 = 8.4, J_2 = 1.2), 8.85 (5H, m), 8.72 (1H, s), 8.56 (1H, t, J = 1.6), 8.53 (1H, dd, J_1 = 5.5, J_2 = 1.2), 8.49 (1H, dd, J_1 = 5.5, J_2 = 1.2), 8.36 (2H, d, J = 1.6), 8.27 (2H, m), 8.18 (4H, m), 8.05 (1H, m), 7.97 (3H, m), 7.84 (4H, m), 7.65 (2H, m), 7.42 (2H, m), 3.97 (6H, s, COO*Me*). ^{13}C NMR δ_C (acetone-d_6): 165.71 (*C*OOMe), 158.38, 158.11, 154.20, 153.08, 153.06, 153.03, 148.73, 148.49, 139.07, 138.93, 137.71, 136.80, 136.34, 133.11, 133.03, 132.88, 132.36, 131.56, 131.52, 130.70, 128.77, 128.64, 127.85, 127.80, 125.34, 125.26, 124.77, 124.49, 123.19, 122.25, 97.73, 91.31, 90.36, 87.00, 53.04 (COO*Me*). HRMS Calcd for $C_{52}H_{36}F_{12}N_6O_4P_2Ru$: 1055.1480. Found: 1055.1494. Anal. Calcd for $C_{52}H_{36}F_{12}N_6O_4P_2Ru$: C, 52.05; H, 3.02; N, 7.00; Found: C, 51.98; H, 3.12; N, 6.81. **1c**: Yield: 65%. IR (cm^{-1}): 3088 (υC−H(Ar)), 2957 (υC−H(aliph.)), 2208 (υC≡C), 1720 (υC═O), 1605 (υC⋯C(Ar)), 1446, 1271. ^{1}H NMR δ_H (acetone-d_6): 8.93 (2H, m), 8.83 (4H, m), 8.56 (1H, t, J = 1.0), 8.34 (2H, d, J = 1.0), 8.21 (6H, m), 8.09 (5H, m), 7.66 (14H, m), 3.97 (6H, s, COO*Me*).^{13}C NMR δ_C (acetone-d_6): 165.83 (*C*OOMe), 158.67, 158.16, 158.13, 158.07, 157.77, 152.93, 152.86, 152.79, 152.70, 139.20, 139.17, 139.09, 136.84, 133.18, 133.05, 132.97, 132.92, 132.78, 132.44, 130.70, 129.77, 129.18, 128.94, 128.92, 127.01, 125.77, 125.48, 125.46, 124.97, 124.18, 123.76, 122.35, 97.90, 92.47, 91.57, 91.53, 90.04, 88.42, 53.08 (COO*Me*). Anal. Calcd for $C_{58}H_{40}F_{12}N_6O_4P_2Ru$: C, 54.60; H, 3.16; N, 6.59; Found: C, 54.83; H, 3.14; N, 6.16.

3. Spectroscopy. *3.1. UV−Vis Absorbance.* Ground state UV−vis absorbance measurements were performed on a Hewlett-Packard 8453 diode array spectrophotometer. The sensitized films were placed diagonally in a 1 cm square quartz cuvette with acetonitrile. An unsensitized film was used as the reference. Transient absorption measurements were acquired with an apparatus that has been previously described.[13] A Xe lamp was used to probe, and 417 nm light from a D_2-filled Raman shifter pumped by a Nd:YAG Continuum Surelite II

laser was used as the excitation beam. Samples were nitrogen purged for at least 15 min or freeze-pump-thawed prior to flash photolysis studies. Sensitized films were immersed in solutions of acetonitrile, neat or with $LiClO_4$. Each kinetic trace was acquired averaging 60−150 laser pulses. The quantum yields for excited state electron injection into TiO_2 were quantified by comparative actinometry as previously described.[19] A Ru(bpy)$_3$(PF$_6$)$_2$ doped poly(methyl methacrylate), PMMA, thin film, whose optical absorption and physical dimensions were very similar to the sensitized TiO_2 films, was used as the actinometer. The amplitudes of photoinduced absorption changes were converted to concentration changes through Beer's law. A literature value for the difference of $(-1.00 \pm 0.09) \times 10^4$ $M^{-1}cm^{-1}$ at 450 nm between the extinction coefficients of the excited state and of the ground state was used.[20] Quantum yields for injection were measured most accurately by probing at wavelengths that corresponded to isosbestic points between the ground and excited states. The isosbestic points were determined on ZrO_2 films where only the ground and MLCT excited states were observed. The extinction coefficients and absorption spectra of the oxidized rigid-rods were determined by spectroelectrochemical measurements.

3.2. Infrared Spectra. IR spectra of the sensitizers were obtained by depositing two drops of a 1 mM CH_3CN solution of the sensitizer on a Ge or CaF_2 window, allowing the solvent to evaporate. The IR spectra of the TiO_2-bound sensitizers were obtained in a transmission mode with films cast on Ge or sapphire windows or by attenuated total reflectance (ATR) with a Golden Gate Single Reflection Diamond ATR apparatus. In all cases, an unsensitized film acted as the background. The spectra were collected with a Nexus 670 Thermo-Nicolet FTIR or a Mattson Research Series 1 FTIR spectrometer at 4 cm^{-1} resolution.

3.3. Raman Spectra. Raman spectroscopy was carried out by using a HoloLab 5000/Raman Rxn1 Confocal Raman Spectrometer (Kaiser Optical Systems, Inc.) with an Invictus 785 nm laser diode. A Teflon sample holder was used to measure the sensitizers (as powders), and the spectra of the TiO_2-bound sensitizers were obtained on films cast on a Sapphire window.

3.4. Photoluminescence. Corrected photoluminescence (PL) spectra were obtained with a Spex Fluorolog that had been calibrated with a standard tungsten−halogen lamp using procedures provided by the manufacturer. Sensitized films were placed diagonally in a 1 cm square quartz cuvette, immersed in acetonitrile, and purged with nitrogen for at least 15 min. The excitation beam was directed 45° to the film surface, and the emitted light was monitored from the front face of the surface-bound sample and from a right angle in the case of fluid solutions. Photoluminescence quantum yield measurements, ϕ_{PL}, were performed using the optically dilute technique with Ru(bpy)$_3$(PF$_6$)$_2$ in acetonitrile as the actinometer, eq 1.[21]

$$\phi_{PL} = (A_r/A_s)(I_s/I_r)(n_s/n_r)^2\phi_r \quad (1)$$

A_r and A_s were the absorbances of the actinometer and sample, respectively, I_r and I_s were the integrated photoluminescence of the actinometer and sample, respectively, n_r and n_s were the refraction indexes for the solvents used for the actinometer and sample, respectively, and ϕ_r was the quantum yield for Ru(bpy)$_3$(PF$_6$)$_2$ in acetonitrile ($\phi_r = 0.062$).[22]

Time-resolved photoluminescence decays were acquired in a similar optical arrangement with excitation from a nitrogen-pumped dye laser that has been previously described.[23] For solution studies, the traces were fit to a first order kinetic model. Values for radiative and nonradiative constants, k_r and k_{nr} respectively, were calculated from eqs 2 and 3 with the measured quantum yields and lifetimes.

$$\phi_{PL} = k_r/(k_r + k_{nr}) \quad (2)$$

$$\phi_{PL} = k_r\tau \quad (3)$$

4. Electrochemistry. Cyclic voltammetry was performed in 0.1 M tetrabutylammonium perchlorate ($TBAClO_4$) CH_3CN electrolyte in a standard three-electrode arrangement with a glassy carbon or sensitized TiO_2 working electrode, a Pt gauze counter electrode, and Ag/AgCl or SCE as the reference electrode. A BAS model CV-50W potentiostat was used, and the CV experiments were carried out at room temperature under argon.

5. Adsorption Isotherms. Surface binding was monitored spectroscopically by measuring the change in film and solution absorbance after soaking the film for 12 h in acetonitrile solutions with known concentrations of the sensitizers. In all cases, the surface coverage saturated at high sensitizer concentration. The equilibrium binding for all Ru-rod sensitizers were well described by the Langmuir adsorption isotherm model[24] from which surface binding constants (K_{ad}) were abstracted using eq 4,

$$\frac{[Ru^{II}]_{eq}}{\Gamma} = \frac{1}{K_{ad}\Gamma_0} + \frac{[Ru^{II}]_{eq}}{\Gamma_0} \quad (4)$$

where $[Ru^{II}]_{eq}$ is the equilibrium sensitizer concentration, Γ_0 is the saturation surface coverage, and Γ is the equilibrium surface coverage at a defined molar concentration. Plots of $[Ru^{II}]_{eq}/\Gamma$ versus $[Ru^{II}]_{eq}$ were fitted linearly to obtain the binding constants K_{ad} and surface coverages Γ_o.

TABLE 1: Surface Adduct Formation Constants and Limiting Surface Coverages for Selected Ru Sensitizers

sensitizer	$10^{-5}K_{ad}$, M^{-1}	Γ_o, mol/cm^2
(deeb)Ru(bpy)$_2^{2+}$	2.0 ± 1.0	$5 \pm 2 \times 10^{-8}$
ROD2-bpyRu(bpy)$_2^{2+}$ (**1b**)	1.9 ± 1.0	$7.3 \pm 0.2 \times 10^{-8}$
ROD2-bpyRu(4,4-Cl$_2$bpy)$_2^{2+}$ (**2b**)	3.7 ± 1.2	$3.9 \pm 0.3 \times 10^{-8}$
Ru(4,4-(Cl)$_2$-bpy)$_2$(bpy)$^{2+}$ (**5**)	5.7 ± 1.3	$4.8 \pm 0.4 \times 10^{-8}$

Results

1. Binding to TiO_2 Films. Adsorption isotherms for sensitizer binding to TiO_2 in acetonitrile were measured at room temperature. All equilibrium binding was well described by the Langmuir adsorption isotherm model from which surface adduct formation constants and limiting surface coverages were obtained.[24] The surface coverages for **1a**−**c** and **2a**−**b** were about 10^{-8} mol/cm^2 and were comparable to those obtained for tripodal sensitizers[5] and for Ru complexes directly bound through a dcb (4,4′-(CO$_2$H)$_2$-bpy) ligand.[1a,c] The binding constants, approximately 2×10^5 M^{-1} for **1a**−**c**, were consistently smaller than those observed for the tripodal sensitizers ($\sim 10 \times 10^5$).[5] The surface binding constants for ROD1-bpyRu(bpy)$_2^{2+}$ (**1b**) and ROD1-bpyRu(4,4′-(Cl)$_2$-bpy)$_2^{2+}$ (**2b**) on pH = 1 pretreated TiO_2 films are reported in Table 1. The reference complex for Cl-substituted rods **2a** and **2b**, Ru(4,4′-(Cl)$_2$-bpy)$_2$(bpy)$^{2+}$ (**5**), had no obvious anchoring groups. However, the equilibrium binding constant for **5** was almost the same as that for Ru complexes that have COOMe binding groups, such as (deeb)Ru(bpy)$_2^{2+}$ and rigid-rods **1a** and **1b** (See Supporting Information, Figure S1). Since control experiments showed that [Ru(bpy)$_3$]$^{2+}$ was weakly adsorbed, adsorption in the case of [Ru(4,4′-(Cl)$_2$-bpy)$_2$(bpy)]$^{2+}$ must have been assisted by the presence of the Cl-bpy ligands.

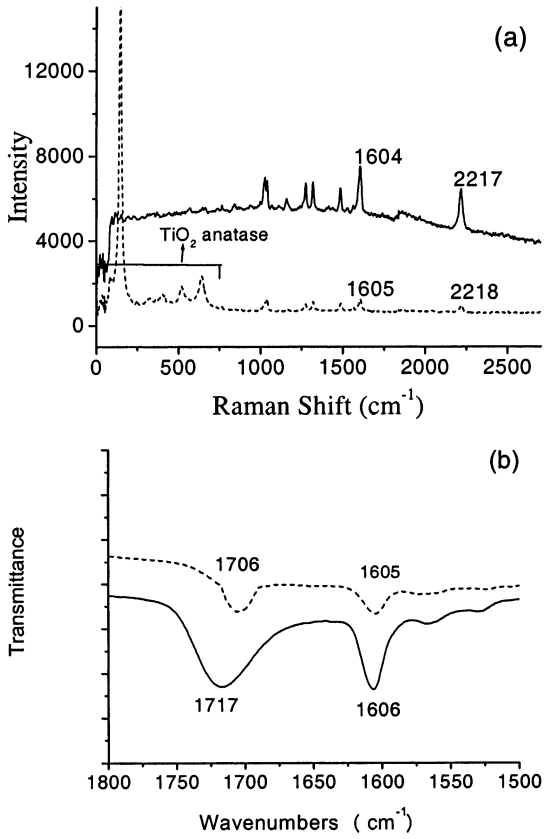

Figure 3. (a) Raman spectra of ester **1a** (—) as a solid and **1a** on TiO_2 (- - -). The TiO_2 film was cast on sapphire and was pretreated with acid. **(b)** IR spectra of the carboxylic acid prepared from ester **1a** (—) on a Ge and **1a** on TiO_2 (- - -). The TiO_2 film was cast on Ge and was pretreated with acid.

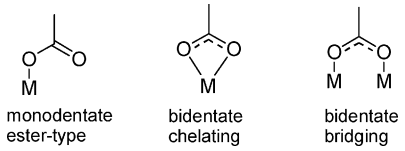

Figure 4. Three possible binding modes for the attachment of a carboxylic group to a metal oxide surface.

2. IR and Raman Spectroscopy. The Raman spectra of **1a** before and after binding differed only from contributions by the characteristic anatase bands, Figure 3a. Both spectra exhibited bands typical of the aromatic ring and of the C≡C bond, but the carbonyl band was too broad and too weak to give reliable information about the surface interaction(s). This was consistent with previous Raman studies of Ru sensitizers on TiO_2.[25] IR measurements were performed for the rigid-rods before and after binding. The pH pretreatment was found to significantly influence the binding process.[14] All spectra of the nonbound esters displayed intense bands at ∼1720 cm^{-1} (νC═O) for the carbonyl and at ∼1600 cm^{-1} (νC⋯C(Ar)) for the phenylene groups. The IR and Raman spectra of **1a** before and after binding to acid-pretreated pH = 1 TiO_2, shown in Figure 3, were representative of the IR and Raman spectra obtained for the rigid-rods. Upon binding to TiO_2 films, the IR spectra exhibited a small (7−12 cm^{-1}) shift to lower wavenumbers of the carbonyl stretch, while the 1600 band due to the aromatic rings remained unchanged, Figure 3b.

Conversely, the IR spectra of the rods bound to basic (pH = 11 pretreated) TiO_2, shown in Figure 5, displayed a broad carboxylate band at ∼1550−1650 cm^{-1}, most consistent with

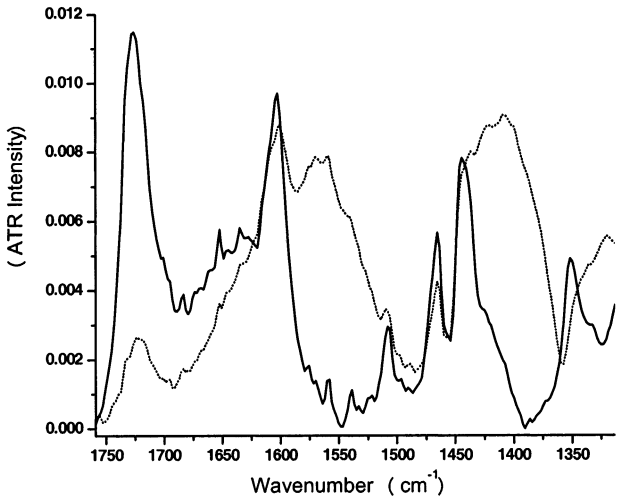

Figure 5. Attenuated total reflectance IR spectra for **2b** on TiO_2 thin films that were pretreated at pH = 1 (—) and pH = 11 (- - -).

bidentate coordination modes as in Figure 4. Interestingly, the rigid-rod sensitizers bound strongly to TiO_2 samples that were *not* pretreated with aqueous acid or basic solutions, and yielded IR spectra with signatures for *both* the carbonyl and the carboxylate band indicative of a mixture of binding modes.

The IR spectra of the rigid-rods obtained on TiO_2 thin films, cast on germanium or sapphire windows, were substrate independent. Germanium was preferred because it combined resistance to aqueous acidic treatments with transparency in the IR region of interest. The presence of a single carbonyl band after binding to an acidic TiO_2 surface suggested that both groups were anchored in a monodentate ester-type bond as in Figure 4.

3. Electrochemistry. All rigid-rod sensitizers displayed quasireversible $Ru^{III/II}$ electrochemistry in CH_3CN electrolyte solution, Table 2. Complexes **1a**, **1b**, and **3** showed $Ru^{III/II}$ reduction potentials at ∼1.3 V versus SCE that were, within experimental error, the same as those reported previously for tripodal sensitizers with $(Ph\text{-}E)_n$ bridges.[5] These waves were shifted to slightly more positive potentials compared to $Ru(bpy)_3^{2+}$. A similar effect was observed in **2a**−**b** and in **5**, as the presence of Cl-substituted ligands resulted in a measurable positive shift in the $Ru^{III/II}$ potential to ∼1.40 V. Ligand-based reduction potentials for the sensitizers in CH_3CN solution are provided in Table 2.

The first reduction, $E°(Ru^{2+/+})$, of **1a**−**c** and **3** occurred at potentials more positive than the corresponding reference complexes, that is, $[Ru(bpy)_3]^{2+}$ or $[Ru(bpy)_2(phen)]^{2+}$, respectively. By comparison with the tripods[5] and with other literature reports on Ru complexes substituted with electron-withdrawing groups,[12,26] we assigned this wave to reduction of the bpy attached to the rigid-rod linker. The presence of 4,4′-$(Cl)_2$-bpy ligands in **2a**−**b** and in **5** resulted first in reduction potentials that were ∼50 mV more positive, consistent with the reduction of the Cl-substituted bpy. The excited state reduction potentials, $E_{1/2}(Ru^{III/II*})$, were calculated from the ground state potentials and from the free energy stored in the thermally equilibrated MLCT excited state, ΔG_{es}, using eq 5:

$$E_{1/2}(Ru^{III/II*}) = E_{1/2}(Ru^{III/II}) - \Delta G_{es} \qquad (5)$$

ΔG_{es} was estimated by drawing a tangent line to the high-energy side of the corrected photoluminescence spectra. The excited state reduction potentials calculated for unsubstituted bpy-based

TABLE 2: Electrochemical Data for 1−3 and Reference Compounds in Solution[a]

complex	$E_{1/2}(Ru^{III/II})$, mV	$E_{1/2}(Ru^{2+/+})$, mV	$E_{1/2}(Ru^{+/0})$, mV	$E_{1/2}(Ru^{III/II*})$, mV
ROD1-bpyRu(bpy)$_2^{2+}$ (**1a**)	1300	−1210	−1480	−820
ROD2-bpyRu(bpy)$_2^{2+}$ (**1b**)	1300	−1230	−1480	−830
ROD3-bpyRu(bpy)$_2^{2+}$ (**1c**)	1287	−1223	−1429	−850
ROD1-bpyRu(4,4-Cl$_2$bpy)$_2^{2+}$ (**2a**)	1400	−1160	−1290	−750
ROD2-bpyRu(4,4-Cl$_2$bpy)$_2^{2+}$ (**2b**)	1390	−1150	−1280	−760
Ru(4,4-(Cl)$_2$-bpy)$_3^{2+}$ (**5**)	1430	−1080	−1190	−730
ROD2-phenRu(bpy)$_2^{2+}$ (**3**)	1300	−1220	−1480	−930
Ru(bpy)$_3^{2+}$ [b] (**4**)	1260	−1340	−1520	−860
[Ru(bpy)$_2$(phen)]$^{2+}$ [b]	1230	−1370	−1530	−910

[a] Data are reported vs SCE. All measurements were performed in 0.1 M $TBAClO_4/CH_3CN$. [b] From Galoppini and co-workers.[5]

TABLE 3: Photophysical Properties of 1−5 and Other Ru Complexes in CH_3CN Solutions[a]

complex	λ_{abs}, nm (ϵ, M^{-1} cm^{-1})[b]	λ_{PL}, nm[c]	τ, μs[d]	ΔG_{es}, eV[f]	$10^2\phi_{PL}$	$10^{-4}k_r$, s^{-1}	$10^{-5}k_{nr}$, s^{-1}
ROD1-bpyRu(bpy)$_2^{2+}$ **(1a)**	462 (1.6×10^4)	640	1.9	2.12	11	5.1	5.4
ROD2-bpyRu(bpy)$_2^{2+}$ **(1b)**	465 (2.0×10^4)	640	2.3	2.13	13	5.4	4.0
ROD3-bpyRu(bpy)$_2^{2+}$ **(1c)**	465 (2.0×10^4)	639	2.5	2.14	9.5	4.7	4.3
ROD1-bpyRu(4,4-(Cl)$_2$-bpy)$_2^{2+}$ **(2a)**	465 (1.6×10^4)	645	0.69	2.15	7.0	10	13
ROD2-bpyRu(4,4-(Cl)$_2$-bpy)$_2^{2+}$ **(2b)**	466 (1.9×10^4)	645	0.75	2.15	6.9	9.2	12
ROD2-phenRu(bpy)$_2^{2+}$ **(3)**	450 (1.8×10^4)	606	1.3	2.23	8.5	6.5	7.0
[Ru(bpy)$_3$]$^{2+}$	450	610	0.80	2.24	6.2	7.8	12
Ru(bpy)$_2$(phen)$^{2+}$	450	620	1.2	2.14			
[Ru(bpy)$_2$(deeb)]$^{2+}$ **(4)**	475 (1.6×10^4)	690	0.93	2.01	4.4	4.7	10
[Ru(4,4-Cl$_2$-bpy)$_3$]$^{2+}$	466	645	0.70	2.16	6.1	8.7	13
[Ru(4,4-Cl$_2$-bpy)$_2$(bpy)]$^{2+}$ **(5)**	461 (1.3×10^4)						
[Ru(bpy)$_2$(bpy-(E-Ph)-AdTripod)]$^{2+}$[g]	461 (1.9×10^4)	646	2.0	2.14	10	5.1	4.5
[Ru(bpy)$_2$(phen-(E-Ph)AdTripod)]$^{2+}$[g]	452 (1.6×10^4)	624	1.4	2.23	8.0	5.7	6.6

[a] All measurements were performed at room temperature. [b] Absorption maxima, ±2 nm. [c] Corrected photoluminescence maxima, ±5 nm. [d] Excited state lifetime in CH_3CN, ±5%. The solutions were deaerated by freeze-pump-thaw or by sparging with nitrogen [e] Half-wave potentials (±20 mV) were measured at a glassy carbon working electrode in 0.1 M $TBAClO_4/CH_3CN$ solution using Ag/AgCl as the reference. Data are reported vs SCE. [f] Gibbs free energy stored in the thermally equilibrated excited state. [g] Data from Galoppini et al.[5b]

rods were nearly identical to those obtained for related bpy-based tripods.[5] Similarly, the potentials for phen-substituted ligand **3** were nearly identical to those obtained for the phen-based tripods.[5] Rigid-rods containing 4,4′-(Cl)$_2$-bpy were weaker excited state reductants by ∼70 mV than those with unsubstituted bpy.

4. Photophysical Studies. Selected photophysical properties for **1**−**5** in argon-saturated acetonitrile at room temperature are listed in Table 3 together with data for the reference complexes and two tripodal sensitizers.

The UV−visible absorption spectra for **1a**−**c**, and for **2a**, **2b**, and **5**, shown in Figure 6, parts a and b, respectively, displayed a broad band in the visible region (400−500 nm) that is typical of metal-to-ligand charge-transfer (MLCT) transitions.

These heteroleptic complexes show broad visible absorption bands and the individual Ru → bpy, Ru → 4,4′-(Cl)$_2$-bpy, or Ru → rigid-rod linker charge transfer bands could not be spectrally resolved. The narrow band at higher energy at ∼290 nm was assigned to the π,π^* transition of the ancillary ligands and the ∼350 nm band was assigned to the π,π^* transition of the rigid-rod (Ph-E)$_n$ linker. As the number of (Ph-E) units increased, the 350 nm band increased in intensity and shifted to longer wavelengths of light. As expected, this band is absent in the spectrum of **5**. The spectral changes were most significant when the number n of (Ph-E)$_n$ units was increased from 1 to 2. As expected, the π,π^* transition at ∼290 nm due to the ancillary bpy was insensitive to the number of (Ph-E) units, Figure 6, parts a and b. Similar spectral features have been observed for the tripodal complexes[4a,5] and oligomeric complexes of Ru.[12,26] A comparison between the absorption maxima for **1a**−**c** and the reference Ru(bpy)$_3^{2+}$ showed an ∼10 nm red shift of the MLCT band in the presence of the linker, while the absorption maxima for **2a**−**b** and the reference complex Ru(4,4′-(Cl)$_2$-bpy)$_3^{2+}$ were identical.[27] The absorption spectra of **1a**−**c** and **3** anchored to TiO_2 and ZrO_2 were largely preserved, with only some minor broadening. The UV spectrum of the reference complex **5b**, however did show an additional shoulder upon binding, possibly due to the Cl−TiO_2 interactions (See Supporting Information, Figure S2).

All the rigid-rod sensitizers displayed room-temperature photoluminescence (PL) in acetonitrile and when anchored to TiO_2 or ZrO_2. The coincident PL maxima for **2a** and **2b** were centered at 645 nm and were identical to that of the [Ru(4,4′-(Cl)$_2$-bpy)$_3$]$^{2+*}$. The PL decays were well described by a first-order kinetic model in fluid solution, and the excited state lifetimes (τ), along with the PL quantum yields, are listed in Table 3. As the number of (Ph-E) increased, for instance from **1a** to **1c**, the τ increased slightly from 1.9 μs ($n = 1$) to 2.3 μs ($n = 2$) and 2.5 μs ($n = 3$). The excited state lifetime for the nonsubstituted complex, Ru(bpy)$_3^{2+}$ is 0.8 μs. Time-resolved PL decays on TiO_2 and on ZrO_2 were nonexponential.[19c]

The transient absorption spectra of the rigid-rods in acetonitrile solutions were assigned to the MLCT excited state. The kinetics were first order, and the rate constants agreed well with the time-resolved PL data at all wavelengths monitored. A comparison of the excited state absorption spectra of **1a**−**c** uncovered distinct differences due the number of (Ph-E) units; **1b** exhibits a stronger, red shifted excited state absorbance beyond 500 nm compared to that of **1a**, Figure 7. The spectra show a bleach of the MLCT absorption, and for **1b** and **1c**, a bleach of the bridge π,π^* transition(s).

The excited state absorption spectra for the Cl-substituted **2a** and **2b** did not display an intense absorption band in the red spectral region and agreed well with the reference complex that lacked the rigid-rod linker, [Ru(4,4′-(Cl)$_2$-bpy)$_3$]$^{2+}$, Figure 8. The excited state absorption spectra obtained on ZrO_2 thin films were within experimental error, the same as that in CH_3CN. Transient absorption spectra on rigid-rod sensitized TiO_2

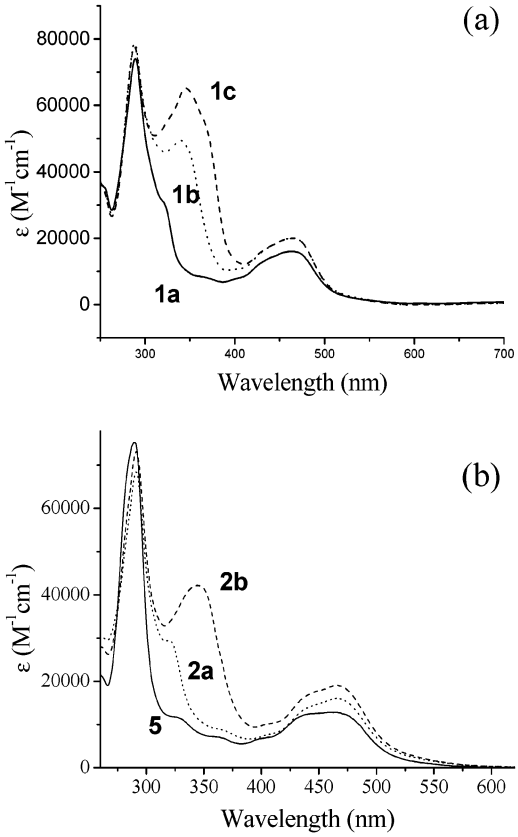

Figure 6. Ground state absorbance spectra in acetonitrile (a) Spectra of **1a** (—), **1b** (···), and **1c** (- - -). (b) Spectra of **2a** (···), **2b** (- - -), and $[Ru(4,4'\text{-}(Cl)_2\text{-}bpy)_2(bpy)]^{2+}$ **5** (—).

contained contributions from the MLCT excited state and from a $Ru^{III}/TiO_2(e^-)$ charge separated state as described below.

5. Interfacial Electron Transfer. Nanosecond transient absorption was used to quantify interfacial electron transfer dynamics and yields. These processes were influenced by the pH. This is expected, since the conduction band edge shifts 59 mV/pH unit.[28,1a] On acidic TiO_2, injection occurred within our instrument response (probably on a femto to picosecond time scale[6]), and the transient spectra were mainly from the $Ru^{III}/TiO_2(e^-)$ charge separated states, while on base pretreated TiO_2 the MLCT excited state was predominately observed. To eliminate possible contributions from the excited state, the measurements were made at wavelengths corresponding to the ground-excited state isosbestic point. In this way, the formation and loss of the interfacial injection and recombination processes could be cleanly observed. On pH = 1 pretreated TiO_2 samples, excited state electron injection into TiO_2 occurred faster than could be time resolved with a nanosecond laser for all samples. On basic TiO_2, the injection yield was very low and could be increased by the addition of $LiClO_4$ to the acetonitrile solution in which the film was immersed. Figure 9 shows absorption changes monitored at the ground-excited state isosbestic point for base pretreated **1a**/TiO_2. The rise time observed corresponds to relatively slow electron injection, $k_{inj} = 1.0 \times 10^7\ s^{-1}$. Typically, 10−30% of the injection process could be observed over the first 100 ns for **1a**−**c**/TiO_2. Injection dynamics were not observed for the rigid-rods anchored to acidic pretreated surfaces, for the reference $[Ru(bpy)_2(deeb)]^{2+}$, or for both Cl-substituted rigid-rod compounds (**2a** and **2b**). The injection is now being studied by femtosecond laser spectroscopy.

Comparative actinometry was used to measure the quantum yields (ϕ_{inj}) for excited state electron transfer to the empty states

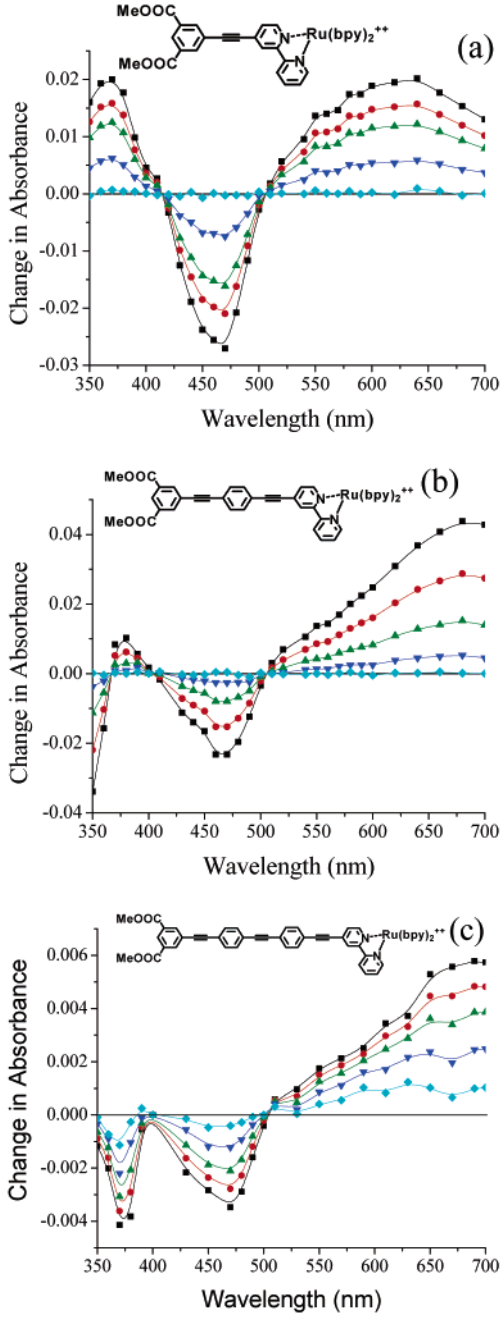

Figure 7. Transient absorbance spectra (λ_{ex} = 417 nm) in CH_3CN of (a) **1a**. The data were recorded at 10 ns (■), 0.5 μs (●), 1.0 μs (▲), 2.0 μs (▼), and 10 μs (◆) delays after the laser pulse. (b) **1b**. The data were recorded at 10 ns (■), 1.0 μs (●), 2.5 μs (▲), 5 μs (▼), and 20 μs (◆) delays after the laser pulse. (c) **1c.** The data were recorded at 0.1 μs (■), 0.5 μs (●), 1.0 μs (▲), 2.0 μs (▼), and 4.0 μs (◆) delays after the laser pulse.

of nanocrystalline TiO_2. The injection yield were found to decrease with irradiance, and extrapolation of the data to zero irradiance gave the ϕ_{inj} reported in Table 4.[19] Injection quantum yields were measured for **1a**−**c** on pH = 1 pretreated TiO_2 and on pH = 11/Li^+ pretreated TiO_2 with comparable surface coverages, $\Gamma(Ru^{II})$. In general, ϕ_{inj} was above 0.60 for Ru−rigid-rod complexes that were bound to pH = 1 pretreated films, while ϕ_{inj} for pH = 11 pretreated films were lower and decreased with rigid-rod length, Table 4.

The kinetics for charge recombination between the electron in TiO_2 and the oxidized sensitizer were quantified on pH = 1 pretreated films at similar surface coverages ($\sim 2.3 \times 10^{-8}$ mol/cm^2). Transient data were obtained at the ground state−excited

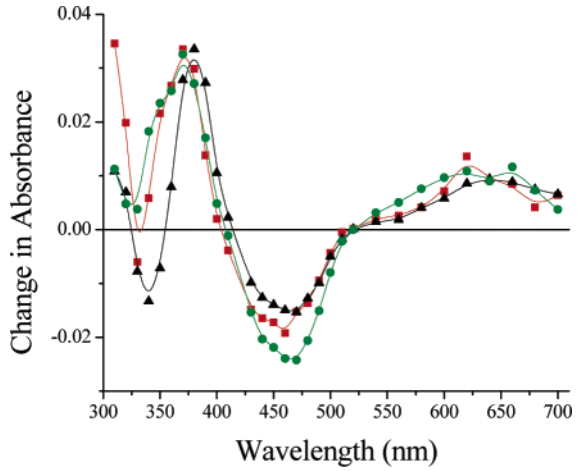

Figure 8. Transient absorbance spectra (λ_{ex} = 417 nm) of Cl-substituted complexes in acetonitrile at room temperature $Ru(4,4'\text{-}(Cl)_2\text{-}bpy)_3(PF_6)_2$ (■), **2a** (●), and **2b** (▲). The data were recorded 10 ns after the laser pulse.

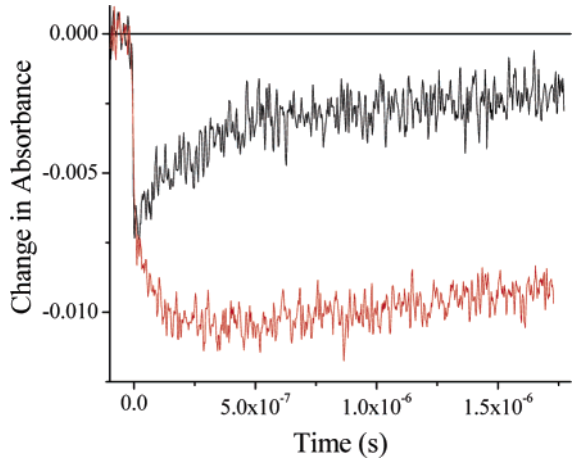

Figure 9. Single wavelength kinetics monitored at the ground state−excited state isosbestic point for **1a** on pH = 1 pretreated TiO_2 (black line, top) and pH = 11 pretreated TiO_2, 0.1 M $LiClO_4$ (red line, bottom).

TABLE 4: Excited State Electron Yields, ϕ_{inj},[a] for Rigid Rods Bound to TiO_2 Films Pretreated with Acid or Base

sensitizer	pH = 1[b]	pH = 11[b]
ROD1-bpyRu(bpy)$_2^{2+}$ (**1a**)	1.0	0.77
ROD2-bpyRu(bpy)$_2^{2+}$ (**1b**)	0.89	0.20
ROD3-bpyRu(bpy)$_2^{2+}$ (**1c**)	0.86	<0.05[c]

[a] All injection yields were measured spectroscopically at room temperature, λ_{exc} = 532.5 nm. [b] The TiO_2 thin film pretreatment prior to binding of the rigid-rod sensitizers. pH = 1 pretreated samples were studied in neat acetonitrile; pH = 11 pretreated films were studied in 0.1 M $LiClO_4$ in acetonitrile. [c] Li^+ addition caused some desorption, so this value was measured in neat acetonitrile.

state isosbestic point to avoid possible contributions from the excited states. The transient data was well described by a bi-second-order kinetic model, eq 6:[19c]

$$\Delta A = \frac{\Delta A_0 - \Delta A_s}{1 + (k_f/\Delta\epsilon l)\, t(\Delta A_0 - \Delta A_s)} + \frac{\Delta A_s}{1 + (k_s/\Delta\epsilon l)\, t(\Delta A_s)} \quad (6)$$

where ΔA was the absorbance change at time t, $\Delta\epsilon$ was the molar extinction coefficient, l was the optical path length, ΔA_0 was the initial amplitude (equal to the sum of the contributions from the fast and slow components), k_f was the recovery rate constant for the fast component, ΔA_s was the amplitude of the slow component, and k_s was the recovery rate constant of the slow component. The average rate constants for charge recombination were found to be independent of the length of rigid-rod sensitizer used and were within experimental error the same as that for the model complex $Ru(bpy)_2(dcb)^{2+}$. The weights of the two components, ~70% and ~30% for the fast and slow components, respectively, were also independent of the length of the rigid-rod sensitizer, with $k_{obs} = 2.5 \pm 0.3 \times 10^7\ s^{-1}$.

Discussion

The photophysical and interfacial electron transfer properties of Ru(II) rigid-rod sensitizers were quantified at room temperature in acetonitrile solution. The interfacial pH was found to be important for both sensitizer binding and for photoinduced electron transfer. Efficient electron injection was observed on acidic TiO_2, while long-lived excited states were observed on basic TiO_2. Back electron transfer rate constants were found to be independent of the length of the rigid-rod excited, consistent with a previously proposed mechanism wherein transport of the injected electron to the oxidized sensitizer was rate limiting.[30] These studies provide new details on surface binding, molecular excited states, and interfacial electron injection. Below we discuss interpretations and implications of these new findings.

1. Surface Binding. Adsorption isotherms and IR studies of the rigid-rod sensitizers **1**−**3** have shown that all bind strongly to nanocrystalline TiO_2 films. In most studies, the methyl esters of the Ru rigid-rods were reacted with the TiO_2 surface in acetonitrile at room temperature. The observation of strong binding was interesting, considering that identical rigid-rod linkers capped with an organic chromophore (pyrene) bound only when it was first converted into a carboxylate salt or a carboxylic acid.[8] Tripodal sensitizers behaved similarly: tripods capped with organic chromophores such as pyrene or perylene did not bind strongly under conditions where Ru tripods did.[31,8] The fact that noncharged, aromatic sensitizers required different binding conditions than the charged Ru complexes may have been due to a variety of factors, such as differences in the solubility in organic solvents and/or electrostatic interactions with the TiO_2 surface.

Infrared measurements showed that both ester groups reacted with TiO_2 to yield a single binding mode whose chemical nature was dependent on the Brønsted acidity of the surface. On acidic TiO_2 surfaces, a single asymmetric CO stretch was observed at higher energy than the methyl ester, which we assigned to ester linkages. On basic TiO_2, a broad band centered at ~1550−1575 cm^{-1} was observed at lower energy and was assigned to a carboxylate binding mode. The fact that only a single binding mode was present on acidic and on basic TiO_2 indicated that both anchoring groups were in a similar environment. Interestingly, on surfaces that were not pretreated with acid or base, spectroscopic signatures of both binding modes were present. We should emphasize, however, that the IR and surface binding studies do not demonstrate that the rigid-rods are perpendicular to the surface or that they assumed a single orientation.

Ruthenium model compounds that contained the $4,4'\text{-}(Cl)_2$-bpy ligand(s) without obvious anchoring groups were found to bind surprisingly well to TiO_2. The rigid-rods that contain $4,4'\text{-}(Cl)_2$-bpy ligands, that is, **2a** and **2b,** may bind with the $Ru(4,4'\text{-}(Cl)_2\text{-}bpy)_2$ "head-down" and the anchoring groups of the linker, all interacting with the TiO_2 surface. This geometry clearly raises issues in the study of remote MLCT states, as discussed later. In addition, the appearance of this unexpected kind of Cl···TiO_2-surface binding stresses the need to carefully evaluate the role of "nonbinding" groups introduced on sensitizers to tune excited state and energetic properties.

2. ^{3}MLCT Excited State in Solution and Surface Bound. The Ru rigid-rods have metal-to-ligand charge-transfer (MLCT) excited states.[27] For the parent compound $Ru(bpy)_3^{2+}$, the preponderance of data supports a "localized" formalism for the thermally equilibrated excited state in fluid solution, that is, $Ru^{III}(bpy^-)(bpy)_2^{2+*}$ not $Ru^{III}(bpy^{-1/3})^{2+*}$.[2,32] Furthermore, for compounds that contain different diimine ligands, the excited state is expected to localize on the ligand that is most easily reduced.[27] It was therefore of interest to consider which ligand-(s) the emissive excited state was localized upon. A second and not completely unrelated issue concerns the extent of charge transfer into the rigid-rod linker.

The $(Ph\text{-}E)_n$ bridge in the rigid-rod linker and the 4,4′-$(Cl)_2$-bpy are known to be electron withdrawing and were therefore expected to stabilize the MLCT excited states.[12,26] This expectation was realized and it is clear that the π^* orbitals of the ligands decrease in energy: bpy > rigid-rod bpy ∼ rigid-rod phen > 4,4′-$(Cl)_2$-bpy. Therefore, the emissive excited state of Ru rigid-rod compounds that contain the 4,4′-$(Cl)_2$-bpy ligand was localized on this ligand, and this explains why their photophysical properties were nearly independent of the Ph-E bridge. For the unsubstituted bpy based Ru rigid-rods, the excited state was localized on the bpy (or phen) attached to the Ph-E bridge. The spectroscopic data reveal the same localized excited states for the rigid-rods in fluid acetonitrile solution and when anchored to ZrO_2 or TiO_2 nanoparticles. Therefore, for the Ru-$(bpy)_2$ rigid-rods, the thermally equilibrated excited state was localized on rigid-rod linkers bound to the semiconductor surface.

It was of interest to compare $Ru(bpy)_2$ rigid-rods where the excited state was localized on a bpy with a variable length phenyl ethyne bridge, **1a**−**c**. The visible absorption and photoluminescence spectra of these rigid-rods were within experimental error the same. Interestingly, the excited state lifetime increased for the two longer rigid-rods relative to the shortest one. For a series of closely related Ru compounds, an increase in lifetime is generally accompanied by a blue shift in the emission spectra in accordance with the energy gap law.[27] The increased lifetime observed here must have a different origin and may reflect the phenylethyne substituents whose extended π conjugation allows for greater electron delocalization. Excited state delocalization disperses the electron into the (Ph-E) bridge, thereby decreasing the average bond displacement energy, which decreases vibrational overlap and hence the nonradiative rate constant.[29]

An alternative explanation for the long-lived "red" emissive excited state is that mixing between MLCT and intraligand excited state(s) of the rigid-rod imparts more triplet character and hence, a longer lived excited state. A mechanism where the MLCT excited state transfers energy to a lower-lying triplet state of the rigid rod is ruled out by the wavelength independent lifetimes measured by transient absorption spectroscopy and the MLCT-like steady state PL spectrum. Nevertheless, excited state delocalization and/or mixing between the MLCT manifold and intraligand triplet states likely explain the long-lived excited state behavior that does not follow the energy gap law.

Indirect evidence for delocalization into the phenylethyne bridge is seen by the strong excited state absorption in the >600 nm region. The first extension of the bridge (from **1a** to **1b**) resulted in significant changes in the intensity and spectrum, while further elongation resulted in smaller differences. Previous researchers have also observed intense near-IR absorption bands for phenylethyne substituted bpy ligands coordinated to Ru(II) and have also attributed this to delocalization of the excited state.[12]

3. Excited State Electron Injection into TiO_2. The quantum yield for excited state injection from the Ru rigid-rods to TiO_2 (ϕ_{inj}), listed in Table 4, was measured on acid (pH = 1) and base (pH = 11) pretreated TiO_2 films on the nanosecond time scale and therefore may not be the true injection yields as any sub-nanosecond (geminate) recombination of the injected electron with the oxidized dye were unaccounted for. Therefore, the ϕ_{inj} values reported here are best considered as lower limits of the true injection yields. The ϕ_{inj} on acid (pH = 1) pretreated TiO_2 were near unity, consistent with negligible geminate recombination. The ϕ_{inj} values for **1a**−**c** decreased by about 15% as the number of (Ph-E) units in the bridge increased. This effect may be due to the increasing distance of the complex from the surface.

At present, however, is not possible to determine whether this is a "distance dependent" effect, since the orientation of the rods with respect to the surface is unknown. Even if both COOR anchoring groups bind to the surface, the axis of the rod may not be perpendicular to the surface and the molecules may bind at an angle (or angles) with respect to the surface. In conclusion, the effective injection distance is unknown and it is probably less than the Ru-center-to-O-bound-to-TiO_2 distance calculated assuming that the molecules are perpendicular (d(**1a**) ∼ 12 Å, d(**1b**) ∼ 19 Å, d(**1c**) ∼ 25 Å).

On base (pH = 11) pretreated TiO_2, the injection yields were very low, $\phi_{inj} < 0.05$, Table 4. This is expected, as the conduction band edge shifts 59 mV/pH unit, resulting in poor orbital overlap with the excited state sensitizer.[28] It is known, however, that the addition of "potential determining ions", such as Li^+, can shift the conduction band edge and promote electron injection under these conditions.[33]

A curious detail of the injection process is that the quantum yield decreased with increased incident irradiance. This behavior was first reported by Kay and Grätzel and was attributed to trap filling that shifts the quasi-Fermi level of TiO_2 toward the vacuum level, making electron injection less favorable.[34] If this explanation were correct, the photoluminescence quantum yield should increase as ϕ_{inj} decreases. However, here, and in previous studies, we find that both quantum yields decrease with irradiance, indicating that some other fast process is lowering the injection yield.[19c]

The electron injection rate constants on acid pretreated TiO_2 films could not be time resolved with the nanosecond laser used in this study ($k_{inj} \gg 10^8$ s^{-1}). This result was expected, since the rates of photoinduced interfacial electron transfer for Ru(II) sensitized TiO_2 are known to occur on the femto to picosecond time scale.[35] Recent ultrafast measurements of tripodal sensitizers 15−24 Å long bound to TiO_2 revealed that the injection occurs on a femto to picosecond time scale.[6,35] We note that injection rate constants $k_{inj} \gg 10^8$ s^{-1} with ($k_r + k_{nr}$) ∼ 5×10^5 s^{-1} for the rods imply that the injection quantum yields should be near unity, consistent with the actinometry measurements.

A fraction of the injection process for the rigid-rods with bpy as the ancillary ligand could be time resolved on base pretreated TiO_2 films immersed in 0.1 M $LiClO_4$ acetonitrile solution. As mentioned above, at basic pH the electron injection is less favorable. Under these conditions, approximately 70−90% of the signal was instrument response limited, while the remaining fraction could be quantified ($k_{inj} \sim 1 \times 10^7$ s^{-1}). This is in agreement with the quantum yields measurements and strongly

suggests that the density of acceptor states for basic TiO_2 is significantly lower than for acidic TiO_2.

The injection rate could not be time resolved, $k_{inj} > 10^8\ s^{-1}$, for the rigid-rods containing the 4,4′-$(Cl)_2$-bpy ancillary ligand bound to acidic as well as basic TiO_2, despite the fact that they are weaker excited state photoreductants than rigid-rods **1a**−**c**. This finding supports the notion that the 4,4′-$(Cl)_2$-bpy ligands interact directly with the TiO_2 surface, and that the molecules may bind "head down", thereby providing a new pathway for electron injection.

In summary, a small fraction of the injection process could be observed on the nanosecond time scale when the TiO_2 was base pretreated *and* when the excited state was localized on a rigid-rod linker. All other experimental conditions led to instrument response limited electron injection rate constants with nearly quantitative yields. The faster and more efficient electron injection into acidic TiO_2 was attributed to a higher density of unfilled states that overlap with the excited state sensitizer orbitals. Femtosecond laser spectroscopy studies aimed to quantify the injection rates for **1a**−**c** to determine whether there are differences due to the linker's length are in progress.

4. Back Electron Transfer. A specific goal of this study was to find conditions where the injection yield was unity while the back electron transfer rate constant decreased with distance. The recombination between the electrons in TiO_2 and the oxidized dye can lower the efficiencies of solar cells. Hence, an attractive way to minimize this process would be to increase the distance between the TiO_2 surface and the metal center, thereby decreasing the rate of recombination. This effect was not realized. Back electron transfer rate constants were found to be independent of the length of the rigid-rod excited. We note that a similar observation was made for the tripodal sensitizers, where the recombination rates between the electrons in TiO_2 and the oxidized dye were found to be independent of the linker's length.[5,6] Recombination of the injected electron with the oxidized dye required milliseconds for completion, and the kinetics were well described by a sum of two second order rate constants. Average rate constants for the rigid-rods **1a**−**c** were within experimental error the same. This is not unexpected in view of literature reports proposing a mechanism wherein transport of the injected electron to the oxidized sensitizer is the rate limiting step.[30] The main process responsible for controlling the recombination rates is usually assumed to be the electron transport by diffusion between trap sites on a semiconductor nanoparticle surface (the Random Flight Model[30]). It is generally concluded that the recombination reaction is governed by the energy redistribution of the electrons trapped in the semiconductor, rather than by spatial diffusion. However, Clifford et al.[36] have recently observed slower recombination dynamics with single exponentials in dye cations that are physically separated from the surface, an effect that is being studied by Tachiya et al.[37] The recent interest in the processes that regulate the recombination rates shows the importance of having available model linkers such as the ones studied here. Based on these data,[36,37] we anticipate observing a distance dependence with TiO_2 materials that have a lower density of trap states and at higher excitation irradiances. Studies of this type will be performed soon.

Conclusions

New rigid-rods Ru(II) polypyridyl complexes were synthesized and anchored to nanocrystalline TiO_2 films for dye sensitization studies. In the rods having unsubstituted bpy as ancillary ligands, the $(Ph\text{-}E)_n$ bridge acts as a π acceptor group, resulting in delocalization of the MLCT state on the linkers, as indicated by measurable spectral shifts in the absorption, PL, and transient absorption spectra. When the ancillary ligands contain Cl groups, there is clear evidence that the MLCT is localized on the 4,4′-Cl_2-bpy. An unexpectedly strong binding between the 4,4′-Cl_2-bpy and the TiO_2 was observed, so that while the rigid-rods bind exclusively through the carboxylic group, the rigid-rods with Cl-substituted ligands may also bind with the Ru complex "head down". Ester-like or carboxylate binding modes to the TiO_2 surface were observed, and conditions to obtain only one type of binding mode were found. The rigid-rods were expected to exhibit diminished electronic coupling with the TiO_2 acceptor states relative to complexes that are directly attached. This behavior was realized under conditions where the density of TiO_2 acceptor states was intentionally decreased by surface pretreatments with basic aqueous solutions. Future studies will focus on ultrafast spectroscopic measurements aiming at quantifying the electron injection process and on the application of these new Ru rigid-rod sensitizers in regenerative solar cells.

Acknowledgment. E.G. and G.J.M. are grateful to the Division of Chemical Sciences, Office of Basic Energy Sciences, Office of Energy Research, U.S. Department of Energy for grant support (DE-FG02-01ER15256 and DE-FG02-96ER14662, respectively).

Supporting Information Available: General Section for the experimental procedures, surface adduct formation plots for **1b**, **2b** and **5**, absorbance spectra of **1a** and **5** in acetonitrile solutions and bound to TiO_2 films. This material is available free of charge via the Internet at http://pubs.acs.org.

References and Notes

(1) (a) Kalyanasundaram, K.; Grätzel, M. *Coord. Chem. Rev.* **1998**, *177*, 347. (b) Hagfeldt, A.; Grätzel, M. *Chem. Rev.* **1995**, *95*, 49. (c) Kamat, P. V. *Chem. Rev.* **1993**, *93*, 267. (d) Qu, P.; Meyer, G. J. In *Electron Transfer in Chemistry*; V. Balzani, Ed.; John Wiley & Sons: New York, 2001; Chapter 2, Part 2, Vol. IV, pp 355−411. (e) Nozik, A. J. *Annu. Rev. Phys. Chem.* **2001**, *52*, 193. (f) Adams, D. M.; Brus, L. C.; Chidsey, E. D.; Creager, S.; Creutz, C.; Kagan, C. R.; Kamat, P. V.; Lieberman, M.; Lindsay, S.; Marcus, R. A.; Metzger, R. M.; Michel-Beyerle, M. E.; Miller, J. R.; Newton, M. D.; Rolison, D. R.; Sankey, O.; Schanze, K. S.; Yardley, J.; Zhu X. Y. *J. Phys. Chem. B* **2003**, *107*, 6668.

(2) Juris, A.; Balzani, V.; Barigelletti, F.; Campagna, S.; Belser, P.; Von Zelewsky, A. *Coord. Chem. Rev.* **1988**, *84*, 85.

(3) Galoppini, E. *Coord. Chem. Rev.* **2004**, *248*, 1283.

(4) (a) Wei, Q.; Galoppini, E. *Tetrahedron* **2004**, *60*, 8497. (b) Guo, W.; Galoppini, E.; Rydja, G. I.; Pardi, G. *Tetrahedron Lett.* **2000**, *41*, 7419.

(5) (a) Galoppini, E.; Guo, W.; Qu, P.; Meyer, G. J. *J. Am. Chem. Soc.* **2001**, *123*, 4342. (b) Galoppini, E.; Guo, W.; Zhang, W.; Hoertz, P. G.; Qu, P.; Meyer, G. J. *J. Am. Chem. Soc.* **2002**, *124*, 7801.

(6) Piotrowiak, P.; Galoppini, E.; Wei, Q.; Meyer, G. J.; Wiewiór, P. *J. Am. Chem. Soc.* **2003**, *125*, 5278.

(7) (a) Wang, D. Ph.D. Thesis, Rutgers University, 2004. (b) Wang, D.; Schlegel, J. M.; Galoppini, E. *Tetrahedron* **2002**, *58*, 6027.

(8) Hoertz, P. G.; Carlisle, R. A.; Meyer, G. J.; Wang, D.; Piotrowiak, P.; Galoppini, E. *Nano Lett.* **2003**, *3*, 325.

(9) Clifford, J. N.; Palomares, E.; Nazeeruddin, Md. K.; Grätzel, M.; Nelson, J.; Li, X.; Long, N. J.; Durrant J. R. *J. Am. Chem. Soc.* **2004**, *126*, 5225.

(10) Argazzi, R.; Bignozzi, C. A.; Hasselmann, G. M.; Meyer, G. J. *Inorg. Chem.* **1998**, *37*, 4533−4537.

(11) Kilså, K.; Mayo, E. I.; Kuciauskas, D.; Villahermosa, R.; Lewis, N. S.; Winkler, J. R.; Gray, H. B. *J. Phys. Chem. A* **2003**, *107*, 3379.

(12) (a) Walters, K. A.; Dattelbaum, D. M.; Ley, K. D.; Schoonover, J. R.; Meyer, T. J.; Schanze, K. S. *Chem Commun.* **2001**, 1834. (b) Li, Y.; Whittle, C. E.; Walters, K. A.; Ley, K. D.; Schanze, K. S. *MRS Symposium Series* **2002**, *665*, 61. (c) Walters, K. A.; Ley, K. D.; Cavalheiro, C. S. P.; Miller, S. E.; Gosztola, D.; Wasielewski, M. R.; Bussandri, A. P.; Van Willigen, H.; Schanze, K. S. *J. Am. Chem. Soc.* **2001**, *123*, 8329. (d) Liu, Y. Li, Y.; Schanze, K. S. *J. Photochem. Photobiol., C* **2002**, *3*, 1. (e) Wang, Y.; Liu, S.; Pinto, M. R.; Dattelbaum, D. M.; Schoonover, J. R.; Schanze, K. S. *J. Phys. Chem. A* **2001**, *105*, 11118.

(13) Heimer, T. A.; D'Arcangelis, S. T.; Farzad, F.; Stipkala, J. M.; Meyer, G. J. *Inorg. Chem.* **1996**, *35*, 5319.
(14) (a) Galoppini, E.; Wang, D.; Chu, D.; Mendelsohn, R. manuscript in preparation. (b) Qu, P.; Meyer, G. J. *Langmuir* **2001**, *17*, 6720.
(15) Hoertz, P. G.; Ph.D. Thesis, Johns Hopkins University, 2003.
(16) Wenkert, D. Woodward, R. B. *J. Org. Chem.* **1983**, *48*, 283.
(17) (a) Hissler, M.; Connick, W. B.; Geiger, D. K.; McGarrah, J. E.; Lipa, D.; Lachicotte, R. J.; Eisemberg, R. *Inorg. Chem.* **2000**, *39*, 447. (b) Mlochowski, J. *Roczniki Chem. Ann. Soc. Chim. Polonorum* **1974**, *48*, 2145.
(18) Sprecher, M.; Breslow, R.; Uziel, O.; Link, T. M. *Org. Prep. Proced. Int.* **1994**, *26*, 696.
(19) (a) Bergeron, B. Meyer, G. J. *Langmuir* **2003**, *19*, 8389. (b) Kelly, C. A.; Farzad, F.; Thompson, D. W.; Meyer, G. J. *Langmuir* **1999**, *15*, 731. (c) Kelly, C. A.; Thompson, D. W.; Farzad, F.; Stipkala, J. M.; Meyer, G. J. *Langmuir* **1999**, *15*, 7047.
(20) Yoshimura, A.; Hoffman, M. Z.; Sun, H. *J. Photochem. Photobiol., A* **1993**, *70*, 29.
(21) Demas, J. N.; Crosby, G. A. *J. Phys. Chem.* **1971**, *75*, 991.
(22) Casper, J. V.; Meyer, T. J. *J. Am. Chem. Soc.* **1983**, *105*, 5583.
(23) Castellano, F. N.; Heimer, T. A.; Tandhasetti, T.; Meyer, G. J. *Chem. Mater.* **1994**, *6*, 1041.
(24) Langmuir, I. *J. Am. Chem. Soc.* **1918**, *40*, 1361.
(25) Keis, K.; Lindgren, J.; Lindquist, S., Hagfeldt, A. *Langmuir* **2000**, *16*, 4688.
(26) (a) Albano, G.; Belser, P.; De Cola, L.; Gandolfi, M. T. *Chem. Commun.* **1999**, 1171. (b) Schlicke, B.; DeCola, L.; Belser, P.; Balzani, V. *Coord. Chem. Rev.* **2000**, *208*, 267.
(27) (a) Meyer, T. J. *Pure Appl. Chem.* **1986**, *58*, 1576. (b) Kober, E. M.; Caspar, J. V.; Lumpkin, R. S.; Meyer, T. J. *J. Phys. Chem.* **1986**, *90*, 3722.
(28) (a) Clark, W. D. K.; Sutin, N. *J. Am. Chem. Soc.* **1977**, *99*, 4676. (b) Watson, D. F.; Marton, A.; Stux, A. M.; Meyer, G. J. *J. Phys. Chem. B* **2003**, *107*, 10971.
(29) Strouse, G. F.; Schoonover, J. R.; Duesing, R.; Boyde, S.; Jones, W. E.; Meyer, T. J. *Inorg. Chem.* **1995**, *34*, 473.
(30) (a) Hasslemann, G. M.; Meyer, G. J.*J. Phys. Chem. B* **1999**, *103*, 7671. (b) Nelson, J. *Phys. Rev. B* **1999**, *59*, 15374. (c) Nelson, J.; Haque, S. A.; Klug, D. R.; Durrant, J. R. *Phys. Rev. B* **2001**, *63*, 205321. (d) Haque, S. A.; Tachibana, Y.; Klug, D. R.; Durrant, J. R. *J. Phys. Chem. B* **1998**, *102*, 1745. (e) Haque, S. A.; Tachibana, Y.; Willis, R. L.; Moser, J. E.; Gratzel, M.; Durrant, J. R. *J. Phys. Chem. B* **2000**, *104*, 538. (f) Barzykin, A. V.; Tachiya, M. *J. Phys. Chem. B.* **2002**, *106*, 4356.
(31) Liu, A., M.S. Thesis, Rutgers University, Newark, 2003.
(32) Dallinger, R. F.; Woodruff, W. H. *J. Am. Chem. Soc.* **1979**, *101*, 4391.
(33) (a) Redmond, G.; Fitzmaurice, D. *J. Phys. Chem. B* **1993**, *97*, 1426. (b) Enright, B.; Redmond, G.; Fitzmaurice, D. *J. Phys. Chem. B* **1994**, *98*, 6195.
(34) Kay, A.; Humphrey-Baker, R.; Grätzel, M. *J. Phys. Chem.* **1994**, *98*, 8, 952.
(35) (a) Zimmermann, C.; Willig, F.; Ramakrishna, S.; Burfeindt, B.; Pettinger, B.; Eichberger, R.; Stork, W. *J. Phys. Chem. B* **2001**, *105*, 9245. (b) Tachibana, Y.; Moser, J. E.; Grätzel, M.; Klug, D. R.; Durrant, J. R. *J. Phys. Chem.* **1996**, *100*, 20056. (c) Haque, S. A.; Tachibana, Y.; Klug, D. R.; Durrant, J. R. *J. Phys. Chem. B* **1998**, *102*, 1745. (d) Asbury, J. B.; Ellingson, R. J.; Ghosh, H. N.; Ferrere, S.; Nozik, A. J.; Lian, T. J. *J. Phys. Chem. B* **1999**, *103*, 3110. (e) Benkö, G.; Kallioinen, J.; Korppi-Tommola, J. E. I.; Yartsev, A.; Sundström, V. *J. Am. Chem. Soc.* **2002**, *124*, 489. (f) Asbury, J. B.; Hao, E.; Wang, Y.; Lian, T. *J. Phys. Chem. B* **2001**, *105*, 4545. (g) Heimer, T. A.; Heilweil, E. J. *J. Phys. Chem. B* **1997**, *101*, 10990. (h) Kasciauskas, D.; Monat, J. E.; Villahermosa, R.; Gray, H. B.; Lewis, N. S.; McCusker, J. K. *J. Phys. Chem. B.* **2002**, *106*, 9347.
(36) Clifford, J. N.; Palomares, E.; Nazeeruddin, Md. K.; Grätzel, M.; Nelson, J.; Li, X.; Long, N. J.; Durrant J. R. *J. Am. Chem. Soc.* **2004**, *126*, 5225.
(37) Barzykin, A. V.; Tachiya, M. *J. Phys. Chem. B* **2004**, *108*, 8385.